Supplementary Material
Shear and bulk acceleration viscosities in simple fluids

Johannes Renner,[1] Matthias Schmidt,[1] and Daniel de las Heras[1]

[1] *Theoretische Physik II, Physikalisches Institut, Universität Bayreuth, D-95440 Bayreuth, Germany*

(Dated: January 28, 2022)

The Supplementary Material contains the expression for the temporal contribution of the current, (A), the description of the calculation of the kernel parameters (B), details about molecular (C) and Brownian (D) dynamics simulations, summaries of the custom flow method (E), the splitting of internal forces into viscous and structural contributions (F) and power functional theory (G), as well as supplementary data on the shear flow in Brownian dynamics (H) and on the traveling shear wave (I).

A. Time evolution of the current

The temporal contribution to the current, shown in Fig.1(a) of the main text, is set to

$$J_t(t) = \begin{cases} 0.5\left[1-\cos\left(\pi t/t_\uparrow\right)\right], & 0 < t \leq t_\uparrow \\ 1, & t_\uparrow < t \leq t_c \\ 0.5\left[1+\cos\left(\pi\frac{t-t_c}{t_\downarrow - t_c}\right)\right], & t_c < t \leq t_\downarrow \\ 0, & t_\downarrow < t, \end{cases} \tag{S1}$$

with $t_\uparrow = 1\tau$, $t_c = 5\tau$, and $t_\downarrow = 6\tau$.

B. Calculation of the kernel parameters

To obtain the memory times and the amplitudes of the viscosity kernels we proceed as follows. For the bulk and the shear flows considered here, the one-body density is by construction time-independent $\rho(\mathbf{r},t) = \rho(\mathbf{r})$ and the one-body current $\mathbf{J}$ factorizes into time- and space-dependent parts $\mathbf{J}(\mathbf{r},t) = \mathbf{J}_\mathbf{r}(\mathbf{r})J_t(t)$. Hence, the time derivative of the current also factorizes into time- and space-dependent parts

$$\dot{\mathbf{J}}(\mathbf{r},t) = \mathbf{J}_\mathbf{r}(\mathbf{r})\dot{J}_t(t), \tag{S2}$$

and it has the same spatial form $\mathbf{J}_\mathbf{r}(\mathbf{r})$ as the current itself. Since the expressions for the shear $\mathbf{f}_s$ and bulk $\mathbf{f}_b$ viscous forces are linear in both $\mathbf{v} = \mathbf{J}/\rho = J_t\mathbf{J}_\mathbf{r}/\rho$ and $\mathbf{a} = \dot{\mathbf{v}}$ where here $\dot{\mathbf{v}} = \dot{\mathbf{J}}/\rho = \dot{J}_t\mathbf{J}_\mathbf{r}/\rho$ [see Eqs. (1) and (2) of the main text], the viscous forces also factorize into time- and space-dependent parts:

$$\mathbf{f}_\alpha(\mathbf{r},t) = C_\alpha(t)\mathbf{f}_{\mathbf{r},\alpha}(\mathbf{r}), \quad \alpha = b, s, \tag{S3}$$

where the space-dependent parts are

$$\mathbf{f}_{\mathbf{r},b} = \frac{1}{\rho}\nabla\left[\rho\rho\nabla\cdot\left(\frac{\mathbf{J}_\mathbf{r}}{\rho}\right)\right], \tag{S4}$$

$$\mathbf{f}_{\mathbf{r},s} = -\frac{1}{\rho}\nabla\times\left[\rho\rho\nabla\times\left(\frac{\mathbf{J}_\mathbf{r}}{\rho}\right)\right], \tag{S5}$$

and the temporal parts are

$$C_\alpha(t) = \int_0^t dt'\left(K_\alpha^\mathbf{v}(t-t')J_t(t') + K_\alpha^\mathbf{a}(t-t')\dot{J}_t(t')\right), \tag{S6}$$

with $\alpha = b$ for bulk and $\alpha = s$ for shear. The kernels are

$$K_\alpha^\mathbf{\Gamma}(t) = \frac{c_\alpha^\mathbf{\Gamma}}{\tau_\alpha^\mathbf{\Gamma}}\exp(-t/\tau_\alpha^\mathbf{\Gamma}), \tag{S7}$$

with the superscript $\mathbf{\Gamma}$ labeling either the acceleration $\mathbf{\Gamma} = \mathbf{a}$ or the velocity $\mathbf{\Gamma} = \mathbf{v}$ contributions. The factorization of the viscous force into temporal- and spatial parts, Eq. (S3), which facilitates the analysis of the data, is not general and holds only if the one-body current also factorizes. Custom flow is therefore an essential tool here since it allows to carefully prescribe the features of the flow. We show in Supplementary Fig. 1 the space-dependent parts of the bulk and shear viscous forces at different times according to simulations. As expected, the curves for different times collapse into a single curve.

The process to calculate the kernel parameters uses two steps. In step one, at every time t we compare the simulation data for $\mathbf{f}_\text{vis}$ to Eq. (S3) using the expressions in Eqs. (S4) and (S5) for the spatial part of the viscous forces. As a result, we obtain the curve $C_\alpha(t)$ in simulations. In the second step, the kernel parameters are obtained by finding the values of $c_\alpha^\mathbf{\Gamma}$ and $\tau_\alpha^\mathbf{\Gamma}$ in Eq. (S6) that best reproduce the curve $C_\alpha(t)$ that results from step one.

C. Molecular dynamics simulations

We use molecular dynamics (MD) to simulate a dynamical ensemble of $\sim 10^6$ instances of a three-dimensional system consisting of $N = 50$ particles interacting via the purely repulsive Weeks-Chandler-Andersen interparticle-interaction potential [1]

$$\phi(r_{ij}) = \begin{cases} 4\epsilon\left[\left(\frac{\sigma}{r_{ij}}\right)^{12} - \left(\frac{\sigma}{r_{ij}}\right)^{6}\right] & \text{if } r_{ij} \geq r_c \\ 0 & \text{otherwise.} \end{cases} \tag{S8}$$

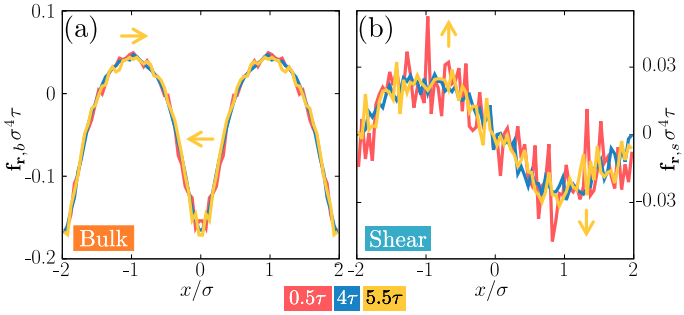

Supplementary Figure 1. Space-dependent parts of (a) the bulk $\mathbf{f}_{\mathbf{r},b}$ and (b) the shear $\mathbf{f}_{\mathbf{r},s}$ viscous forces as a function of the x-coordinate obtained with MD simulation data. Three different times are shown, as indicated by the color of the lines. The arrows indicate the direction of the vector field at the selected positions.

Here, $r_{ij} = |\mathbf{r}_i - \mathbf{r}_j|$ is the distance between particle i and j, and $r_c = 2^{\frac{1}{6}}\,\sigma$ is the cutoff radius, which is located at the minimum of the Lennard-Jones potential. We work in units of the length scale σ, the energy scale ϵ, and the mass of one particle m. Hence, the derived time scale is $\tau = \sqrt{m\sigma^2/\epsilon}$.

The equations of motion for the ith particle are

$$\frac{d\mathbf{r}_i}{dt} = \frac{\mathbf{p}_i}{m}, \tag{S9}$$

$$\frac{d\mathbf{p}_i}{dt} = -\nabla_i u(\mathbf{r}^N) + \mathbf{f}_{\text{ext}}(\mathbf{r}_i, t), \tag{S10}$$

where $\mathbf{r}_i$ denotes the position of the ith particle, and $\mathbf{p}_i = m\mathbf{v}_i$ its momentum, with $\mathbf{v}_i$ its velocity. The total force acting on the particle is made of an external contribution $\mathbf{f}_{\text{ext}}(\mathbf{r}_i, t)$, and an internal one, $-\nabla_i u(\mathbf{r}^N)$. Here, ∇_i is the partial derivative with respect to $\mathbf{r}_i$ and $u(\mathbf{r}^N) = \frac{1}{2}\sum_i \sum_{j\neq i} \phi(r_{ij})$ is the total interparticle potential energy with, $\mathbf{r}^N = \{\mathbf{r}_1 \dots \mathbf{r}_N\}$ the complete set of particle positions.

We integrate the many-body equations of motion in MD using the standard velocity-Verlet algorithm with time step $dt = 10^{-4}\tau$. The simulation box is a cuboid with lengths $L_x = 4\sigma$, $L_y = 10\sigma$ and $L_z = 8\sigma$ and periodic boundary conditions. To spatially resolve the one-body fields we discretize the system in the x-coordinate with bins of size 0.05σ.

The particle positions are initialised randomly with the constraint that no interparticle interaction occur. The particle velocities are initialised following a Maxwell-Boltzmann distribution with absolute temperature T. For the initial equilibration of the shear flow (homogeneous density) we let the system evolve for $1\,\tau$ without external force. To initialize the compressible flow (inhomogeneous density profile), we use custom flow to grow the density inhomogeneity and then let the system equilibrate for $4\,\tau$ such that memory effects decay. The starting temperature, calculated from the kinetic energy using the equipartition theorem, is set to $k_BT/\epsilon = 0.59$ (compressible flow) and $k_BT/\epsilon = 0.486$ (shear flow). Here, k_B is the Boltzmann constant. The temperatures of the final equilibrium states are $k_BT/\epsilon = 0.60$ and $k_BT/\epsilon = 0.492$ for the compressible and the shear flows, respectively. These values are slightly higher than the initial values due to the heating induced by the external driving. Since the temperature increase was small (below 2%) we did not use a thermostat. Note however that custom flow can also be implemented together with a thermostat [2].

The one-body fields of interest are resolved in space and in time. For example, the one-body density and current profiles are given by

$$\rho(\mathbf{r}, t) = \left\langle \sum_{i=1}^{N} \delta\left(\mathbf{r} - \mathbf{r}_i\right) \right\rangle, \tag{S11}$$

$$\mathbf{J}(\mathbf{r}, t) = \left\langle \sum_{i=1}^{N} \delta(\mathbf{r} - \mathbf{r}_i)\mathbf{v}_i \right\rangle, \tag{S12}$$

with $\delta(\mathbf{r})$ being the three dimensional Dirac delta distribution, and $\mathbf{r}$ being the position vector. The statistical average, denoted by the brackets $\langle\cdot\rangle$ is done at each time t over different realizations of the initial conditions (the positions and the velocities of the particles at the initial time $t = 0$). Specifically, we average over $2 \cdot 10^6$ different realizations (initial states).

D. Brownian dynamics simulations

For the overdamped Brownian dynamics simulations we use the standard Euler algorithm to integrate the equation of motion of the ith particle

$$\mathbf{r}_i(t + dt) = \mathbf{r}_i(t) + \frac{dt}{\gamma}[-\nabla_i u(\mathbf{r}^N) + \mathbf{f}_{\text{ext}}(\mathbf{r}_i, t)] + \boldsymbol{\eta}_i(t), \tag{S13}$$

where $\boldsymbol{\eta}_i$ is a delta-correlated Gaussian random displacement with standard deviation $\sqrt{2dtk_BT/\gamma}$ in accordance with the fluctuation-dissipation theorem and γ is the friction coefficient against the (implicit) solvent. We hence use in Eq. (S13) the standard assumption that the random force does not depend on the external force [3]. The integration time step is set to $dt = 10^{-4}\tau_b$ with $\tau_b = \sigma^2\gamma/\epsilon$ the BD unit of time. In BD we work in units of σ, ϵ, and γ. We average over $4 \cdot 10^6$ trajectories, i.e. twice than in MD, due to the larger statistical noise generated by the random force. The velocity of particle i at time t, required to e.g. sample the current following Eq. (S12), is calculated as the central derivative of the position vector [4]:

$$\mathbf{v}_i(t) = \frac{\mathbf{r}_i(t + dt) - \mathbf{r}_i(t - dt)}{2dt}. \tag{S14}$$

All further parameters of the simulation, i.e. temperature, number of particles, and target fields, are the same as in MD.

Since the external driving is time-dependent, the overdamped approximation that underlies Eq. (S13) might

not be accurate. However, we use here overdamped BD only as a reference system in which inertial effects are eliminated by construction. This allows us to highlight the inertial effects that occur in MD.

E. Custom flow

Custom flow is a numerical method that finds the external force corresponding to prescribed density, velocity, and acceleration fields (the target fields). A complete description of the method is given in Refs. [2, 4]. Here, we only summarize the main ideas of custom flow in molecular dynamics. The external force is found iteratively. At each iteration, the external force is the same as in the previous iteration plus a term that aims to correct the differences between sampled and target fields,

$$\mathbf{f}_{\text{ext}}^{(k+1)}(\mathbf{r},t) = \mathbf{f}_{\text{ext}}^{(k)}(\mathbf{r},t) + \frac{m}{\rho(\mathbf{r},t)\Delta t}\left(\mathbf{J}(\mathbf{r},t) - \mathbf{J}^{(k)}(\mathbf{r},t)\right). \tag{S15}$$

Here, k is the iteration index. Hence, $\mathbf{f}_{\text{ext}}^{(k)}(\mathbf{r},t)$ and $\mathbf{J}^{(k)}(\mathbf{r},t)$ denote the external force and the current sampled at iteration k, whereas $\rho(\mathbf{r},t)$ and $\mathbf{J}(\mathbf{r},t)$ are the target fields. The convergence of the iteration scheme (S15) is achieved when the external forces at iterations $k+1$ and k coincide within a given tolerance (in practice less than ten iterations are usually enough to achieve convergence). The whole iteration scheme needs to be repeated at time intervals separated by Δt which we set to be $\Delta t = 10dt$, i.e., ten times bigger than the time step of the simulation dt. At each time, we initialize the external force according to

$$\mathbf{f}_{\text{ext}}^{(0)}(\mathbf{r},t) = \frac{m\dot{\mathbf{J}}(\mathbf{r},t)}{\rho(\mathbf{r},t)}, \tag{S16}$$

which follows from the exact one-body force balance equation (S30) by making the internal force $\mathbf{f}_{\text{int}}$ and the transport term $\nabla\cdot\boldsymbol{\tau}$ zero everywhere.

Using Eq. (S15), custom flow MD minimizes the difference between target and sampled one-body currents. This results in very accurate (essentially noise free) sampled currents. The noise, which in standard MD simulations usually occurs in the sampled fields, appears in custom flow in the external force which is tailored to the initial set of microstates (we use $2\cdot 10^6$ different initial states), see Supplementary Figure 2. For a better visual representation we show in the main paper and also in Supplementary Figure 2 smooth external force profiles which result from removing the high Fourier modes of the raw signal. Both, the external force that follows directly from custom flow and its smoothed version produce very similar dynamics [2].

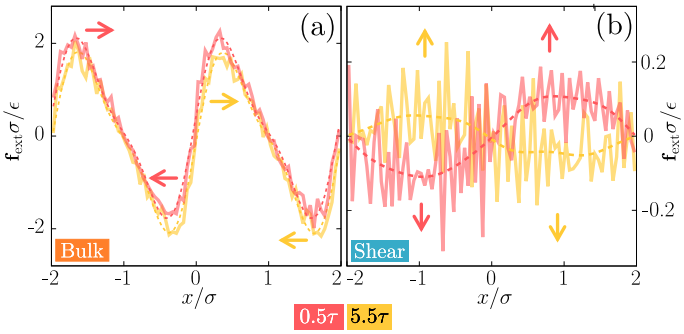

Supplementary Figure 2. External force $\mathbf{f}_{\text{ext}}$ produced by MD custom flow (solid thick lines) as a function of x for (a) bulk and (b) shear flows at times 0.5τ (red) and 5.5τ (yellow). The smoothed external forces, obtained by removing the high frequency modes, are also shown with dashed lines. Custom flow minimizes the statistical noise that usually occurs in the sampled fields like the density and the velocity profiles. As a result, the external forces obtained with custom flow appear to be noisy. The colored arrows indicate the direction of the force at the selected positions.

F. Viscous and structural internal forces

In non-equilibrium, the total internal force $\mathbf{f}_{\text{int}}$, which is solely generated by the interparticle interactions, contains structural and flow contributions [5]. The structural part is able to e.g. sustain gradients in the density profile, whereas the flow contribution represents the viscous response of the system. The total internal force is easily accessible in computer simulations since $\mathbf{f}_{\text{int}}(\mathbf{r},t) = \mathbf{F}_{\text{int}}(\mathbf{r},t)/\rho(\mathbf{r},t)$ with $\mathbf{F}_{\text{int}}$ being the internal force density

$$\mathbf{F}_{\text{int}}(\mathbf{r},t) = -\left\langle \sum_{i=1}^{N} \delta(\mathbf{r}-\mathbf{r}_i)\nabla_i u\left(\mathbf{r}^N\right)\right\rangle. \tag{S17}$$

To extract the viscous forces from the total internal force, we use that the viscous forces are sensitive to the direction of the flow. Hence, reversing the direction of the flow, i.e., $\mathbf{v}\to-\mathbf{v}$ and $\mathbf{a}\to-\mathbf{a}$ while keeping the density profile unchanged, flips the sign of the viscous forces and leaves the structural forces unchanged [5]. The sign change of $\mathbf{f}_{\text{vis}}$ by reversing the direction of the flow is apparent in Eqs. (1) and (2) of the main text.

Hence, the total viscous force of the system can be calculated as [5]

$$\mathbf{f}_{\text{vis}}(\mathbf{r},t) = \frac{\mathbf{f}_{\text{int}}(\mathbf{r},t) - \mathbf{f}_{\text{int}}^{r}(\mathbf{r},t)}{2}, \tag{S18}$$

where $\mathbf{f}_{\text{int}}^{r}(\mathbf{r},t)$ indicates the internal force in the reverse system, i.e. a system with flow velocity $-\mathbf{v}(\mathbf{r},t)$, acceleration $-\mathbf{a}(\mathbf{r},t)$, but the same density profile $\rho(\mathbf{r},t)$ as the original forward system [in which the flow is given by $+\mathbf{v}(\mathbf{r},t)$ and $+\mathbf{a}(\mathbf{r},t)$ and the internal force is $\mathbf{f}_{\text{int}}(\mathbf{r},t)$].

Using Eq. (S18) to measure the viscous force is always possible if the density profile is time-independent, such

as e.g. steady states and the full non-equilibrium flows designed here. If the density varies in time, then temporal changes of the density profile affect the flow (via the continuity equation). In such cases finding the reverse system to unambiguously measure the viscous force is in general not possible. This again highlights the importance of custom flow that allows us to generate flows in which the viscous response can be unambiguously measured.

To create the reverse system we follow two independent methods which give the same results. The first method simply uses custom flow to prescribe the respective reverse flow and find the corresponding external force. The second method makes use of symmetry arguments to compute the reverse flow from the forward flow and hence obtain $\mathbf{f}^r_{\rm int}$ from $\mathbf{f}_{\rm int}$. This second possibility, which we describe in detail in what follows, is possible only due to the specific characteristics of the flows. In the general case the first method is required to find the reverse system.

Bulk flow. Let us consider a virtual flow in which we reverse at each time t only the x-component of every particle in the original flow, i.e. we perform the operation $x_i(t) \to -x_i(t)$ while keeping the other two components unchanged. Hence, the x-component of the current in this virtual system, J^v_x, is

$$J^v_x = \left\langle \sum_{i=1}^N \delta(x-(-x_i)) \frac{d(-x_i)}{dt} \right\rangle = -\left\langle \sum_{i=1}^N \delta(x+x_i) v_i^x \right\rangle = -J_x(-x,t). \quad \text{(S19)}$$

By construction, the bulk flow has the symmetry $J_x(x,t) = J_x(-x,t)$. Hence, in combination with Eq. (S19) above we conclude that $J^v_x(x,t) = J^r_x(x,t)$. Also by construction, the other components of the current vanish and the density profile has also the same symmetry $\rho(x,t) = \rho(-x,t)$. Therefore, we can construct the reverse system of the bulk flow by simply using the trajectories of the forward system and performing the operation $x_i(t) \to -x_i(t)$.

Hence, for the bulk flow the x-component of the internal force density in the reverse system is

$$F^r_{\rm int,x}(x,t) = \left\langle \sum_{i=1}^N \delta(x+x_i) \frac{\partial \phi(r_{ij})}{\partial(-x_i)} \right\rangle \quad \text{(S20)}$$

$$= -\left\langle \sum_{i=1}^N \delta(x+x_i) \frac{\partial \phi(r_{ij})}{\partial x_i} \right\rangle \quad \text{(S21)}$$

$$= -F_{\rm int,x}(-x,t), \quad \text{(S22)}$$

where we have used that the interparticle distance r_{ij} is not affected by the transformation $x_i \to -x_i$. Due to the spatial symmetry of the density profile $\rho(x,t) = \rho(-x,t)$, the internal force $\mathbf{f}_{\rm int}$ has the same symmetry as the internal force density $\mathbf{F}_{\rm int}$, i.e. $f^r_{\rm int,x}(x,t) = -f^r_{\rm int,x}(-x,t)$ because $\mathbf{F}_{\rm int} = \mathbf{f}_{\rm int}/\rho$. Therefore, for the bulk flow the viscous part of the total internal force, see Eq. (S18), can be obtained from the forward bulk flow as a simple arithmetic mean

$$f_{{\rm vis},x}(x,t) = \frac{f_{{\rm int},x}(x,t) + f_{{\rm int},x}(-x,t)}{2}. \quad \text{(S23)}$$

Shear flow. Here, the flow is directed along the y-axis and the density is homogeneous $\nabla\rho = 0$. Therefore, by construction, the y-component of the internal force is only of viscous nature (no structural term). We arrive at the same conclusion by considering a virtual flow in which we reverse at each time the y-component of all particles, i.e. $y_i(t) \to -y_i(t)$. Hence, the y-component of the current in the virtual system J^v_y is

$$J^v_y(x,t) = \left\langle \sum_{i=1}^N \delta(x-x_i) \frac{d(-y_i)}{dt} \right\rangle \quad \text{(S24)}$$

$$= -\left\langle \sum_{i=1}^N \delta(x-x_i) v_i^y \right\rangle = -J_y(x,t), \quad \text{(S25)}$$

which is precisely the y-component of the current in the reverse system $J^r_y(x,t) = J^v_y(x,t)$. Given that the other two components of the current vanish and that the density profile is stationary, we conclude that the reverse system can be obtained from the forward flow by simply using the operation $y_i(t) \to -y_i(t)$ and performing the desired averages.

The y-component of the internal force density in the reverse system is therefore

$$F^r_{\rm int,y}(x,t) = \left\langle \sum_{i=1}^N \delta(x-x_i) \frac{\partial \phi(r_{ij})}{\partial(-y_i)} \right\rangle \quad \text{(S26)}$$

$$= -\left\langle \sum_{i=1}^N \delta(x-x_i) \frac{\partial \phi(r_{ij})}{\partial y_i} \right\rangle \quad \text{(S27)}$$

$$= -F_{\rm int,y}(x,t). \quad \text{(S28)}$$

Hence, using Eq. (S18), the viscous part is

$$f_{{\rm vis},y}(x,t) = \frac{f_{{\rm int},y}(x,t) + f_{{\rm int},y}(x,t)}{2} = f_{{\rm int},y}(x,t). \quad \text{(S29)}$$

That is, as expected, the flow-direction of the internal force in a shear flow contains only viscous terms provided that there is no density inhomogeneity in the flow direction.

G. Power functional theory

Power functional theory (PFT) is a variational theory that describes the dynamics of interacting many-body overdamped [6] and inertial [7] systems at the level of one-body fields. A variational principle produces by construction the exact one-body force balance equation of

the system. For a classical system of particles following the equations of motion (S9) and (S10), the exact one-body force balance equation reads [7]

$$m\dot{\mathbf{J}}(\mathbf{r},t) = \rho(\mathbf{r},t)\left[\mathbf{f}_{\rm ext}(\mathbf{r},t) + \mathbf{f}_{\rm int}(\mathbf{r},t)\right] + \nabla\cdot\boldsymbol{\tau}(\mathbf{r},t), \quad \text{(S30)}$$

where the last term involves the divergence of the second rank kinetic stress tensor $\boldsymbol{\tau}$ and it describes transport effects that arise due to the one-body description of the dynamics. In thermal equilibrium this term reduces to diffusive transport $\nabla\cdot\boldsymbol{\tau} = -k_BT\nabla\rho$. In simulations, $\boldsymbol{\tau}$ can be sampled via

$$\boldsymbol{\tau}(\mathbf{r},t) = -m\left\langle \sum_{i=1}^{N}\delta(\mathbf{r}-\mathbf{r}_i)\mathbf{v}_i\mathbf{v}_i \right\rangle, \quad \text{(S31)}$$

where $\mathbf{v}_i\mathbf{v}_i$ indicates the dyadic product of the velocity of particle i with itself.

Within PFT each term of the force balance equation (S30) is generated via a functional derivative of a corresponding functional generator with respect to the time derivative of the current or alternatively with respect to the acceleration field. The density profile ρ, the current $\mathbf{J}$ (or the velocity $\mathbf{v} = \mathbf{J}/\rho$), and the time derivative of the current $\dot{\mathbf{J}}$ (or the acceleration $\mathbf{a} = \dot{\mathbf{v}} = \dot{\mathbf{J}}/\rho$, where the second equality holds only if $\dot{\rho} = 0$ like in the present work) are the natural functional dependencies of the generator functionals. One important task in PFT is to find an approximated functional that generates via functional differentiation the internal force field.

The simplest approximation based on an expansion in terms of the acceleration gradient $\nabla\mathbf{a}$ that is (i) compatible with the symmetry requirements of the viscous force (the force must flip sign under flow reversal) and that (ii) respects the rotational invariance of the system under global rotations is

$$G_b[\rho,\mathbf{v},\mathbf{a}] = \int d\mathbf{r}\int_0^t dt' K_b^{\mathbf{v}}(t-t')\rho'(\nabla\cdot\mathbf{v}')(\nabla\cdot\mathbf{a})\rho + \int d\mathbf{r}\int_0^t dt' K_b^{\mathbf{a}}(t-t')\rho'(\nabla\cdot\mathbf{a}')(\nabla\cdot\mathbf{a})\rho, \quad \text{(S32)}$$

$$G_s[\rho,\mathbf{v},\mathbf{a}] = \int d\mathbf{r}\int_0^t dt' K_s^{\mathbf{v}}(t-t')\rho'(\nabla\times\mathbf{v}')\cdot(\nabla\times\mathbf{a})\rho + \int d\mathbf{r}\int_0^t dt' K_s^{\mathbf{a}}(t-t')\rho'(\nabla\times\mathbf{a}')\cdot(\nabla\times\mathbf{a})\rho, \quad \text{(S33)}$$

where we have omitted the dependencies of the one-body fields, e.g. $\rho = \rho(\mathbf{r},t)$, primed fields are evaluated at t', e.g. $\rho' = \rho(\mathbf{r},t')$, and the spatial integral runs over the whole system. Analogue expressions arise in overdamped Brownian dynamics based on an expansion in terms of the velocity gradient $\nabla\mathbf{v}$ [8].

The shear $\mathbf{f}_s$ and bulk $\mathbf{f}_b$ viscous forces shown in Eqs. (1) and (2) of the main text are then generated via the functional derivative

$$\mathbf{f}_\alpha(\mathbf{r},t) = -\frac{\delta G_\alpha}{\delta\dot{\mathbf{J}}(\mathbf{r},t)} = -\frac{1}{\rho}\frac{\delta G_\alpha}{\delta\mathbf{a}(\mathbf{r},t)}, \qquad \alpha = b,s, \quad \text{(S34)}$$

where the derivative is taken at time t with respect to either $\dot{\mathbf{J}}$ or $\mathbf{a}$ and considering that the fields $\rho(\mathbf{r},t')$, $\mathbf{v}(\mathbf{r},t')$, and $\mathbf{a}(\mathbf{r},t')$ are kept fixed at their real physical values for all previous times $t' < t$. Hence, the functional derivative in Eq. (S34) acts only on the unprimed terms $\mathbf{a}(\mathbf{r},t)$ of Eqs. (S32) and (S33) but not on the primed $\mathbf{a}' = \mathbf{a}(\mathbf{r},t')$ ones.

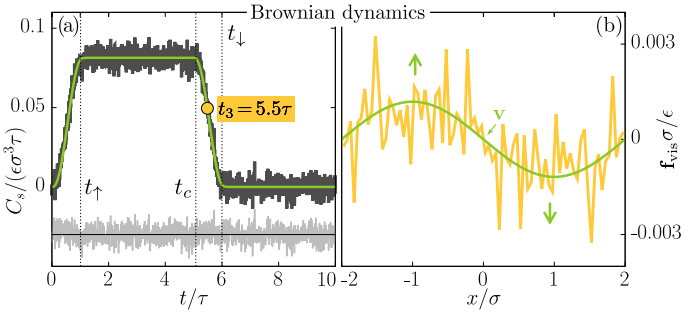

Supplementary Figure 3. (a) Temporal dependency of the shear viscous force C_s as a function of time t in Brownian dynamics simulations (thick black line) and theoretically (green) for the shear flow described in the main text. The vertical dotted lines indicate the times $t_\uparrow, t_c$, and $t_\downarrow$. The time $t_3 = 5.5\tau$ is highlighted with a yellow circle. The light grey line fluctuating around the horizontal line is the difference between simulation (thick black) and theory (violet). (b) Shear viscous force $\mathbf{f}_{\rm vis}$ as a function of x at time $t_3 = 5.5\tau$ according to BD (yellow) and theory (green). The force points along the y-axis. The colored arrows indicate the direction of the force at the selected positions.

H. Shear flow in Brownian dynamics

As in the case of the compressible flow, we have also analysed the shear flow using Brownian dynamics simulations. Since the acceleration field does not play any role in overdamped Brownian dynamics, the velocity field alone reproduces the complete shear viscous force. We show in Supplementary Fig. 3 the temporal part $C_s(t)$ of the viscous force vs time, and the viscous force vs the x-coordinate for a given time obtained in Brownian dynamics simulations along with the corresponding theoretical predictions [kernel parameters $c_s^v/(\epsilon\sigma^3\tau) = 0.081$ and $\tau_s^v/\tau = 0.059$]. The parameters of the flow are identical to those used in MD (see main text).

I. Traveling shear wave

For the traveling shear wave, the current follows up to $t = 2\tau$ the same time evolution as in the shear case, see Eqs. (8) and (9) of the main text. After $t = 2\tau$, the shear

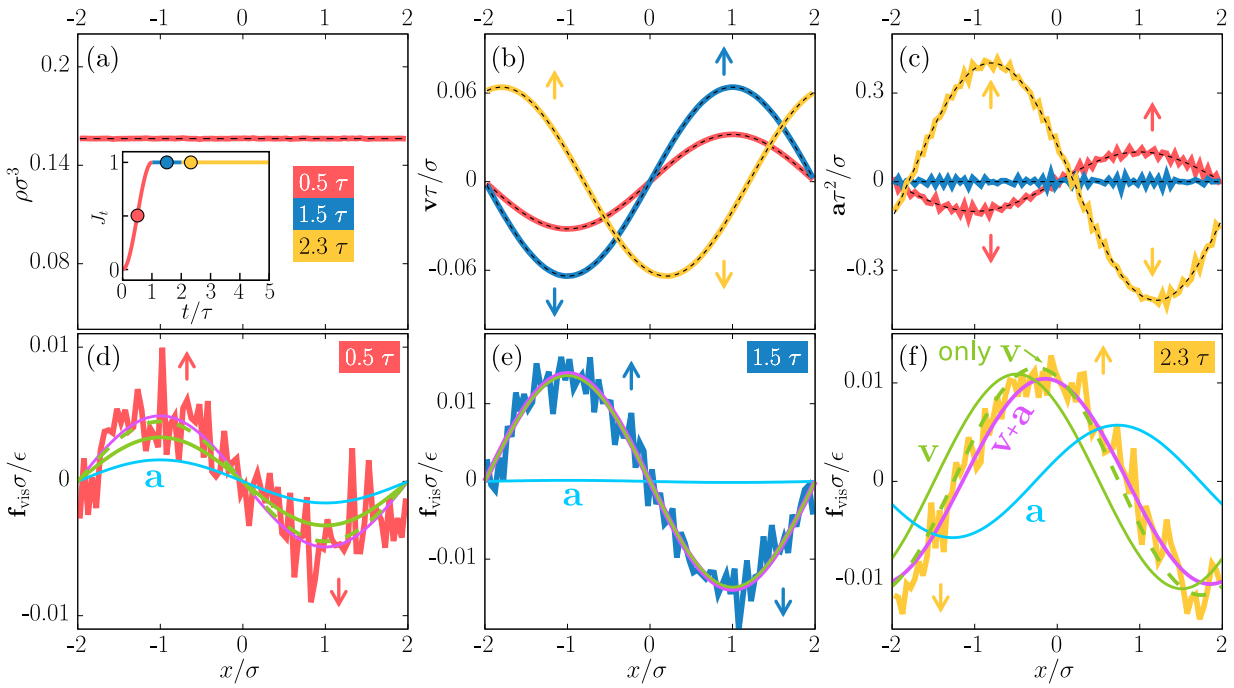

Supplementary Figure 4. Density (a), velocity (b), and acceleration (c) profiles vs the x-coordinate for the shear flow with a traveling wave. Three different times $0.5\,\tau$ (red), $1.5\,\tau$ (blue), and $2.3\,\tau$ (yellow) are shown. Solid lines are simulation data sampled using custom flow and thin black-dashed lines are the corresponding target fields. The inset in (a) shows the temporal dependency of the current with the three different regimes highlighted using different color and the selected times indicated by colored circles. The amplitude of the current increases until $t/\tau = 1$ (red) and then it remains constant until the simulation ends. The shear wave is stationary at first (blue) and then it starts to travel for $t/\tau > 2$ (yellow). Panels (d),(e), and (f) show the shear viscous force at different times (as indicated) obtained in simulations (thick solid lines) along with the theoretical prediction using the acceleration and the velocity contributions (violet) and also using only the velocity contribution (dashed green). The individual contributions of the velocity (solid green) and of the acceleration (blue) to the total signal (violet) are also shown. Once the shear wave is traveling (f) there is a clear phase shift between the simulation data (yellow) and the prediction using only the velocity (dashed green). Using both contributions (violet) the simulation data is correctly reproduced. The color arrows indicate the direction of the respective vector field at the selected positions.

wave starts to move with constant velocity $v_s = 4\sigma/\tau$ and constant amplitude, i.e.

$$\mathbf{J}(\mathbf{r},t) = J_0 \sin\left(\frac{2\pi(x - v_s t)}{L_x}\right)\hat{\mathbf{e}}_y, \quad t > 2\tau, \qquad \text{(S35)}$$

where, as in the non-traveling shear case, $L_x/\sigma = 4$ and $J_0\tau\sigma^2 = 0.01$. Representative states for each of the regimes of the traveling shear flow are shown in Supplementary Fig. 4. The density (a) remains constant in space at every time. The amplitudes of the velocity (b) and of the acceleration (c) increase until $t = 1\tau$. To relax memory effects, the velocity profile remains stationary from 1τ to 2τ. Hence, the acceleration vanishes everywhere in that time period. Then, the traveling wave begins to move and the velocity field changes its phase with constant speed. Therefore, the acceleration field has a constant instantaneous phase shift of $\pi/2$ with respect to the velocity field. This is different from what we considered in the static shear wave and allows us to test our model for the shear viscous force. The shear viscous forces at three different times are shown in panels (d),(e), and (f) of Supplementary Fig. 4. We show the data sampled in molecular dynamics simulations along with the theoretical predictions which we calculate with the same kernel parameters previously obtained for the static shear wave flow. The agreement between simulation and theory is excellent, not only before the wave starts to travel (d,e), which was expected from the static shear case, but also during the traveling wave (f). The phase shift between $\mathbf{v}$ and $\mathbf{a}$ has an effect on the viscous force that is theoretically reproduced. In contrast, if we use only the velocity dependent part of the viscous force and the same kernel parameters as for the static case, there is a phase shift between the theoretical predictions and the simulation data. The acceleration field is therefore required to describe the data accurately.

[1] John D. Weeks, David Chandler, and Hans C. Andersen, "Role of repulsive forces in determining the equilibrium structure of simple liquids," J. Chem. Phys **54**, 5237

(1971).
[2] Johannes Renner, Matthias Schmidt, and Daniel de las Heras, "Custom flow in molecular dynamics," Phys. Rev. Res. **3**, 013281 (2021).
[3] R Kubo, "The fluctuation-dissipation theorem," Rep. Prog. Phys. **29**, 255–284 (1966).
[4] D. de las Heras, J. Renner, and M. Schmidt, "Custom flow in overdamped Brownian dynamics," Phys. Rev. E **99**, 023306 (2019).
[5] Daniel de las Heras and Matthias Schmidt, "Flow and structure in nonequilibrium brownian many-body systems," Phys. Rev. Lett. **125**, 018001 (2020).
[6] M. Schmidt and J. M. Brader, "Power functional theory for brownian dynamics," J. Chem. Phys. **138**, 214101 (2013).
[7] Matthias Schmidt, "Power functional theory for Newtonian many-body dynamics," J. Chem. Phys. **148**, 044502 (2018).
[8] D. de las Heras and M. Schmidt, "Velocity gradient power functional for Brownian dynamics," Phys. Rev. Lett. **120**, 028001 (2018).